minerals

MDPI

Article

Formation of Au-Bearing Antigorite Serpentinites and Magnetite Ores at the Massif of Ophiolite Ultramafic Rocks: Thermodynamic Modeling

Valery Murzin [1], Konstantin Chudnenko [2], Galina Palyanova [3,4,*] and Dmitry Varlamov [5]

1 A.N. Zavaritsky Institute of Geology and Geochemistry, Ural Branch of Russian Academy of Sciences, Akademika Vonsovskogo str., 15, 620016 Ekaterinburg, Russia; murzin@igg.uran.ru
2 A.P. Vinogradov Institute of Geochemistry, Siberian Branch of Russian Academy of Sciences, Favorskogo str., 1a, 664033 Irkutsk, Russia; chud@igc.irk.ru
3 V.S. Sobolev Institute of Geology and Mineralogy, Siberian Branch of Russian Academy of Sciences, Akademika Koptyuga pr., 3, 630090 Novosibirsk, Russia
4 Department of Geology and Geophysics, Novosibirsk State University, Pirogova str., 2, 630090 Novosibirsk, Russia
5 Institute of Experimental Mineralogy, Russian Academy of Sciences, 142432 Chernogolovka, Moscow Region, Russia; dima@iem.ac.ru
* Correspondence: palyan@igm.nsc.ru

Received: 10 October 2019; Accepted: 2 December 2019; Published: 5 December 2019

Abstract: We constructed thermodynamic models of the formation of two types of gold-ore mineralization at the Kagan ultramafic massif in the Southern Urals (Russia). The first type of gold-mineralization is widely spread at the massif in the tectonic zones of schistose serpentinites containing typically ≤ 0.1 ppm Au. The second type of gold-ore mineralization is represented by veined massive, streaky and impregnated magnetite ores in contact with serpentinites. It contains to 5 vol.% sulfides and 0.2–1.2 ppm Au. Our thermodynamic calculations explain the formation of two types of gold-ore mineralization in the bedrocks of ultramafic massifs. Metamorphic water, which is the result of the dehydration of early serpentinites (middle Riphean) during high-temperature regional metamorphism (700 °C, 10 kbar) (late Precambrian), is considered as the source of ore-bearing fluid in the models. The metasomatic interaction of metamorphic fluid with serpentinites is responsible for the gold-poor mineralization of the 1st type at T = 450–250 °C and P = 2.5–0.5 kbar. The hydrothermal gold-rich mineralization of the 2nd type was formed during mixing of metamorphic and meteoric fluids at T = 500–400 °C and P = 2–3 kbar and discharge of mixed fluid in the open space of cracks in serpentinites. The model calculations showed that the dominant forms of gold transport in fluids with pH = 3–5 are $AuCl_2^-$ complexes (≥450 °C) and, as the temperature decreases, $AuHS^0$, or $AuOH^0$. Mineral associations obtained in model calculations are in general similar to the observed natural types of gold mineralization.

Keywords: Kagan ultramafic massif; Southern Urals; antigorite serpentinites; magnetite veins; gold mineralization; native gold; thermodynamic modeling; fluid regime

1. Introduction

The Urals is one of the most important gold provinces in the Russia and in the world [1,2]. By the end of the 20th century, the Urals was one of the five largest regions in the world in gold mining. By that time, about 500 gold deposits of various scales were known [3]. Nowadays, the main proportion of gold is extracted as an accessory component from volcanogenic massive sulfide deposits localized in the Tagilo–Magnitogorskian zone (Figure 1A). These deposits are associated with the upper mantle

basaltoid magmatism. The largest gold-ore deposits (Kochkarskoe, Berezovskoe, Svetlinskoe, etc.) belong to the quartz veined and sulfide disseminated types, occuring within the East Uralian zone, and are related to the products of crustal granitoid magmatism [4]. Haloes of gold-bearing placers are widespread there owing to primary deposits. Massifs of ophiolite mafic-ultramafic rock complexes occur in the Main Uralian Fault zone (MUF). The long-term occurrence of tectonic, metamorphic, and metasomatic processes resulted in a deep transformation of these complexes and the origin of various types of gold-bearing rocks: antigorite serpentinites, rodingites, magnetite-chlorite-carbonate, and other varieties [5–7].

Deposits and ore occurrences in ultramafic massifs (Karabash, Verh-Neivinsk, Talovsk, Kagan, etc.) are scarce. They contain small amounts of the gold, but industrial placers of these occuring metals are widespread throughout the massif. Native gold in these placers is represented by Au–Cu intermetallides, as well as Au–Ag–Cu, Au–Ag, and Au–Ag–Hg solid solutions. Placer gold is larger in size and is frequently intergrown with magnetite, chlorite, pyroxene, and serpentine. The genetic aspects of formation of gold mineralization in ultramafic rocks are problematic and their discussion has started quiet recently [8–13]. This work continues the discussion.

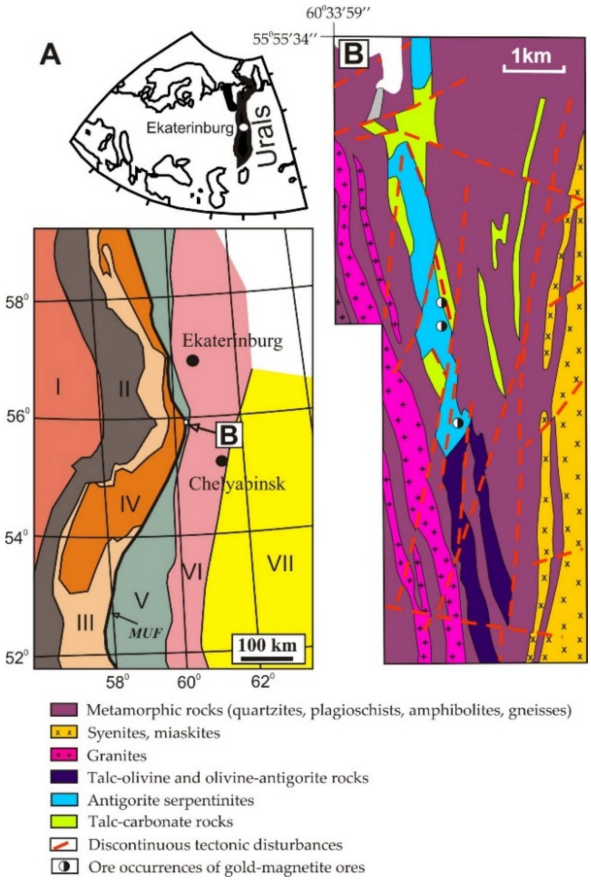

Figure 1. Location of the Kagan massif on the scheme for tectonic structure of the Urals from [4] (**A**); and its geologic structure from [14] (**B**). A—Tectonic zones of the Urals; I—East European platform; II—Preuralian foredeep; III—West Uralian zone; IV—Central Uralian zone; V—Tagilo–Magnitogorskian zone; VI—East Uralian zone; VII—Transuralian zone. MUF—Main Uralian Fault.

The object of our study is gold-bearing serpentinites and their sulfide–magnetite ores at the Kagan ultramafic massif in the Southern Urals (Russia) (Figure 1A). The massif occurs in the Main fault zone within the Sysert–Vishnevogorsk metamorphic complex. Gold-bearing ultramafic rocks and sulfide–magnetite ores of the Kagan massif occur in antigorite serpentinites and were referred to a

gold-productive serpentinite (antigorite) metasomatic formation [7]. Gold-magnetite ore occurrences were exploited in the middle of the 20th century by two small mines.

Based on the results of the previous study [9] of altered rocks from the Kagan massif and gold–sulfide–magnetite ores, a suggestion was made that the metamorphic fluid, which mobilized metals from ultramafic rocks, could be the source of gold and other metals (Fe, Cu, Ag). The aim of this work is to develop physicochemical models of the formation of gold mineralization in the processes of metamorphogenic–metasomatic transformation of ultramafic substance, using computer thermodynamic modeling with the help of the Selektor-C software and available geological, geochemical, mineralogical, and other data on the object under study. Further, in the following section we provide a review of literature data on the studied model object, including published and unpublished results obtained by us. These data were used to construct a thermodynamic model of the object under study.

2. Geological and Metallogenic Overview

2.1. Geological Setting and Types of Gold Mineralization of the Kagan Massif

Premetamorphic ultramafic rocks in the Vishnevogorsk and other metamorphic complexes of the Middle (Sysert) and South (Ilmenogorsk) Urals are distinquished as part of the Riphean ophiolite association developed on the Archean–early Proterozoic basement [14]. Ultramafic and volcano–sedimentary rocks of ophiolite association were metamorphosed under the conditions of subgranulite to upper green–schist facies. A several stages of metamorphic and metasomatic alterations of ultramafic rocks are identified (Table 1). Gold and anthophyllite mineralization occur with them [9,15,16].

Table 1. Stages of metamorphism and metasomatism of ultramafic rocks in the Sysert–Ilmenogorsk metamorphic complex [14] and the types of mineralization associated with them [9,15,16].

Stages of Metamorphism and Metasomatism, Age	Composition of Metamorphic and Metasomatic Rocks (From High to Low Temperature)	Type of Mineralization
Regional zonal dynamothermal metamorphism, Late Precambrian	Enstatite–olivine Talc–olivine Antigorite–olivine Antigorite	Gold–sulfide–magnetite, Gold–antigorite
Regional silicic acid metasomatism, O_2–S_1 Local silicic acid metasomatism, P_3–T	Tremolite–chlorite Enstatite Anthophyllite, tremolite–anthophyllite enstatite–anthophyllite, talc–carbonate–anthophyllite chlorite-biotite, chlorite–actinolite	Gold–sulfide Anthophyllite–asbest

The Kagan massif is a concordant tabular body 400–600 m thick and 16 km long. It occurs in the plagioschists and amphibolites of the middle Riphean in the northwestern wing of the Vishnevogorsk anticline (Figure 1B). To the west of the massif, among metamorphic rocks, there are dikes of plagioclase and two-feldspar granites. In the east, metamorphic rocks make contact with the Vishnevogorsk syenite–miaskite intrusion in the Ilmenogorsk alkaline complex. The metamorphism of the rocks of the Kagan massif is associated with the late Precambrian stage and is manifested in the zoning of the massif. Talc–olivine and olivine–antigorite rocks are developed in the southern part of the massif; to the north they are replaced by antigorite serpentinite with the sites of olivine–antigorite rocks and talc–carbonate rocks (Figure 1B). Silica–acid metasomatism in the Kagan massif is weakly expressed and is manifested in the development of anthophyllite in talc–olivine rocks and talc in olivine–antigorite and antigorite rocks. The periphery parts of the Kagan massif in its narrow zones are transformed into tremolite–anthophyllite rocks [14].

Gold-ore mineralization occurs among antigorite serpentinites in the central and northern parts of the Kagan massif. Its two types are distinguished.

The first type of gold-ore mineralization is widely spread at the massif in the tectonic zones of schistose serpentinites. During the prochispecting and mapping works for gold in 1991, it was revealed that schistose serpentinites of the Kagan massif, tested on drill holes, pits, and ditches, have low contents of gold, typically ≤ 0.1 ppm. Nevertheless, crushed samples frequently contain grains of native gold with a size of 0.05–0.1 mm, less often 0.2–0.35 mm. The mechanisms of enlargement of native gold particles in natural migration processes (dissolution, transfer, and deposition) of noble metal are interpreted in many works [17–21].

The second type of gold-ore mineralization is represented by veined massive, streaky and impregnated magnetite ores (Figure 2) containing to 5 vol.% sulfides. Gold–sulfide–magnetite ores occur in the tectonic zone stretching along the eastern contact of the northern part of the massif for 2 km (Figure 1B). Magnetite lenses are to 5–6 m long and to 0.2 m thick and arranged in chains along the tectonic zone. Assay analysis shows that Au content in such ores is 0.2–1.2 ppm, and it drastically increases in the areas with visible gold. Chemical–spectral analysis also showed the presence of platinum group elements (PGE) (in ppm): to 0.77 Pd, to 0.02 Pt, and to 0.01–0.02 Rh, Ir, Os, and Ru [22]. PGE anomalies are common for many serpentinites [23].

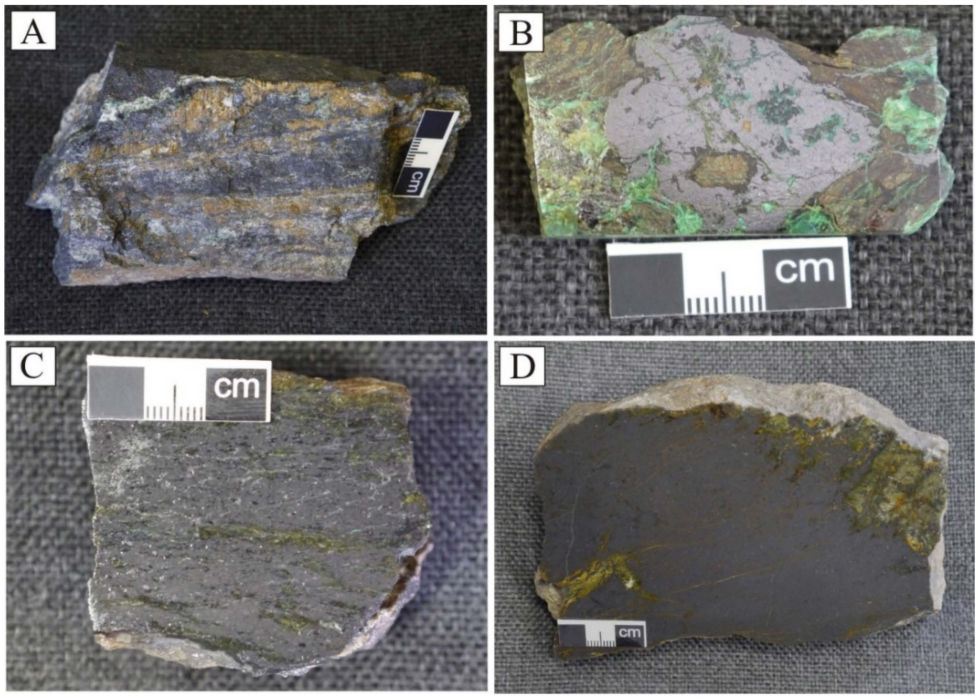

Figure 2. Magnetite ores from Kagan deposit: (**A**) banded ore composed of magnetite and serpentinite bands (brown); (**B**) disseminated ore with oxidation products of copper sulfides (green); (**C**) banded massive ore with bands of serpentinite; (**D**) massive ore (black) in contact with serpentinite.

2.2. Mineralogy of Gold-Bearing Antigorite Serpentinites and Gold–Sulfide–Magnetite Ores

Serpentinites containing native gold are composed of a lamellar aggregate of antigorite with a small amount of talc, chlorite, tremolite, metamorphic olivin (Mg/(Mg + Fe) = 0.96–0.98) as well as relict olivine (Mg/(Mg + Fe) = 0.92–0.93), clinopyroxene, and loop-shaped serpentine. Mg/(Mg + Fe) of relic olivine corresponds to the typical composition of accessory olivine in dunites and harzburgite. Antigorite contains 6.4–12.3 wt % FeO. Its laths are zoned, with its edges richer in iron than the central parts. Talc and chlorite replace antigorite. In serpentinites one can observe scattered grains of Cr–spinel up to 2 mm in size, tiny crystals of magnetite, and rare particles of pentlandite (to 0.5 mm). Cr–spinel is replaced by Cr–magnetite and Cr–clinochlore. Magnetite contains 0.9–1.5 wt % MgO and 0.4–2.0 wt % Cr_2O_3. It is typical for most other serpentinites [24–26].

Tremolite (Mg/(Mg + Fe) = 0.95–0.96) is likely synchronous to antigorite. It develops after clinopyroxene and is actively replaced through the net of thin veinlets by late serpentinite and chlorite of clinochlore–pennine series.

The grains of native gold from antigorite serpentinites have flattened, less often, isometric shapes and sizes up to 0.35 mm. Their chemical composition is given in Table 2 and in Figure 3A. Native gold is characterized by content up to 22.23 wt % Ag and small amounts of 0.2–0.4 wt % Cu. Individual grains contain 0.29–0.78 wt % Cu (average 0.42), one grain 6.5 wt % Cu and 0–1.7 (average 0.17) wt % Hg. The fineness of native gold varies from 772 to 996‰.

Table 2. Chemical composition and fineness of native gold from zones of schistose serpentinites of Kagan massif.

No. Sample/ Grain	Au wt %	Ag wt %	Cu wt %	Hg wt %	Total, wt %	Fineness, ‰ *
K-10/1	99.06	0.04	0.63	0.0	99.73	993
K-10/2	98.98	0.09	0.59	0.0	99.66	993
K-10/10	92.21	0.43	6.52	0.0	99.16	930
K-5/11	85.86	13.93	0.34	0.0	100.13	857
K-6/12	77.41	22.23	0.60	0.0	100.24	772
C-437/13	92.55	5.44	0.21	1.72	99.92	926
Sp-207/14	92.17	8.13	0.26	0.11	100.67	916
Sp-207/15	95.10	4.23	0.36	0.03	99.72	954
Sp-207/16	99.13	0.92	0.31	0.0	100.36	988
Sp-207/17	97.70	2.43	0.78	0.0	100.91	968
Sp-201/18	90.74	9.66	0.29	0.0	100.69	901
Sp-212/19	99.90	0.16	0.47	0.0	100.53	994
Sp-212/20	89.03	9.17	0.33	0.53	99.06	899
Sp-212/21	99.14	0.0	0.41	0.0	99.55	996
Sp-212/22	91.96	8.18	0.29	0.0	100.43	916
Sp-212/23	97.72	1.74	0.78	0.0	100.24	975
Sp-328/1	94.05	5.52	0.42	0.0	99.99	941
Sp-328/25	92.87	6.79	0.41	0.0	100.07	928
Sp-328/26	95.70	4.11	0.52	0.0	100.33	954

Note. * Au × 1000/(Au + Ag + Cu + Hg). Composition was determined in the Institute of Geology and Geochemistry, Ural Branch of RAS on the electron-probe micro analyzer JXA-5a (analyst V.A. Vilisov). Analytical conditions: U = 20 kV, standards are pure metals and HgTe. The average measurement accuracy is 0.3 wt % for Au, Ag, Cu, Pd, and 1 wt % for Hg (which is associated with the possible migration of mercury from the analysis zone).

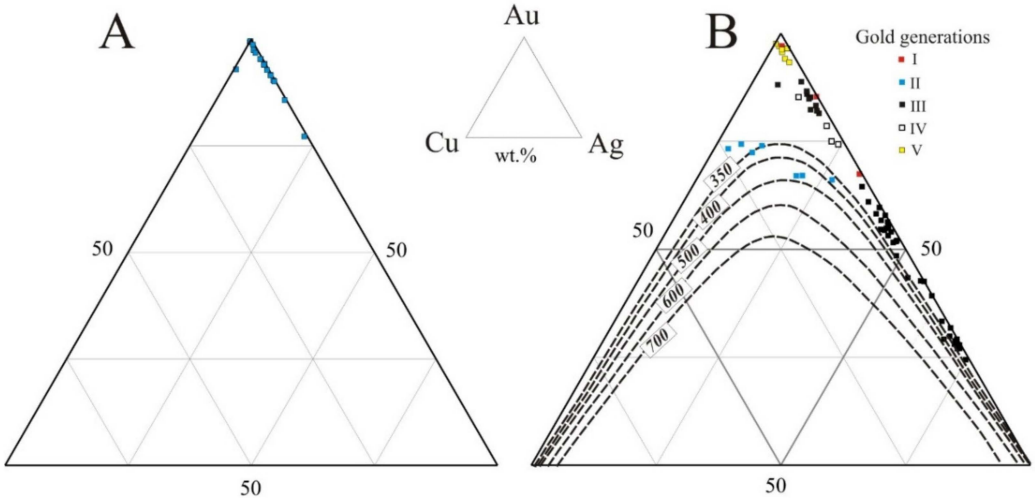

Figure 3. Composition of native gold from Kagan massif on the Au–Ag–Cu diagram: (**A**) from schistose antigorite serpentinites; (**B**) various generations of native gold from magnetite ores. The diagram contains the isotherms (°C) of ternary solid solution from experimental data [27].

Disseminated and massive ores are composed of polygonally grained aggregates of magnetite with grains smaller than 1 mm and a low content of sulfides (no less than 2–5 vol.%). Accumulations of magnetite are cemented with antigorite and minor talc (Mg/(Mg + Fe) = 0.97–0.98), chlorite (Mg/(Mg + Fe) = 0.91–0.95), and tremolite (Mg/(Mg + Fe) = 0.95–0.96). Talc is developed after serpentine (Figure 4A).

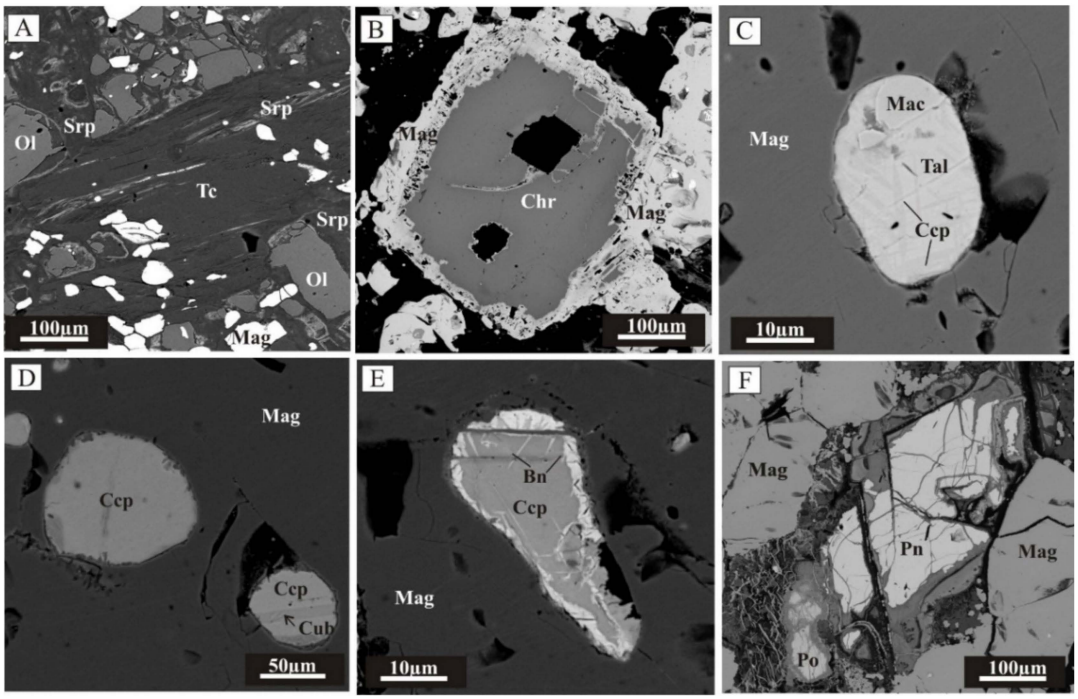

Figure 4. Relationships of minerals in gold–sulfide–magnetite ores: (**A**) development of talc (Tc) after relict olivine (Ol) and serpentine (Srp); (**B**) rim of magnetite (Mag) replacing a grain of relict Cr–spinel (Chr); (**C**,**D**) sulfides of early parageneses: (**C**) grain of talnakhite (Tal) with plates of chalcopyrite (Ccp) and mackinawite (Mac) inclusion in magnetite, (**D**) chalcopyrite inclusions (one of them with plates of cubanite (Cub)) in magnetite; (**E**,**F**) sulfides of late paragenesis: (**E**) inclusion composed of chalcopyrite and bornite (Bn) in magnetite; (**F**) pentlandite (Pn) and pyrrhotite (Po) in magnetite. Here and in Figure 5 are electronic-microscopic images in the regime of back-scattered electrons (BSE).

Among aggregates of antigorite one can also observe Cr–spinel (Cr/(Cr + Al) = 0.56–0.67), olivine (Mg/(Mg + Fe) = 0.92–0.98) and loop-shaped serpentine.

The whole mass of magnetite ore is penetrated by a net of thin veinlets of chrysotile (Mg/(Mg + Fe) = 0.94–0.99), chlorite (Mg/(Mg + Fe) = 0.93 to –0.94) and dolomite.

The groundmass of magnetite from massive and disseminated ores contains 1.0–2.4 wt % MgO. The grains of Cr–spinel present in magnetite ore are replaced by Cr–magnetite and Cr–clinochlore (Figure 4B). The composition of Cr–spinel and Cr–magnetite is uncommon and contains a high amount of MnO (0.4–5.2 wt %) and ZnO (0.1–3.5 wt %).

Sulfides are represented by early and late parageneses. Sulfides of early paragenesis are chalcopyrite $CuFeS_2$, pyrrhotite $Fe_{1-x}S$, talnakhite $Cu_9(Fe,Ni)_8S_{16}$, cubanite $CuFe_2S_3$, and Cu-, Co-bearing mackinawite $(Fe,Ni)_9S_8$ (Figure 4C,D). These sulfides form rounded inclusions less than 50 μm in size in magnetite. Sulfides of late paragenesis are chalcopyrite $CuFeS_2$, bornite Cu_5FeS_4, pyrrhotite $Fe_{1-x}S$, Co-pentlandite $(Fe,Ni)_9S_8$, and Fe-sphalerite ZnS. They are localized in the intergranular space among aggregates of magnetite and form segregations to 2–3 mm in size (Figure 4E,F). Sulfides of both parageneses contain inclusions of native gold.

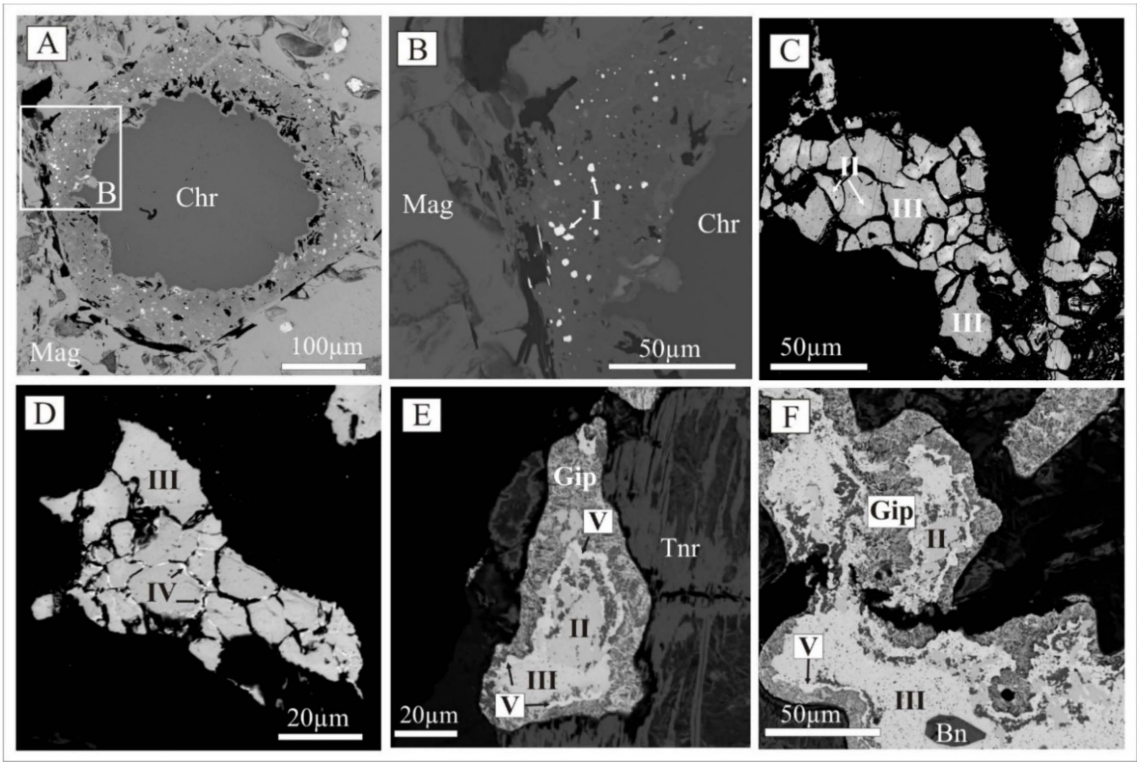

Figure 5. Native gold of generations I–V from magnetite ores of Kagan massif: (**A**) inclusions of native gold of generation I and copper sulfides in magnetite (Mag) replacing Cr–spinel (Chr); (**B**) fragments on "a"; (**C**) aggregates of zoned grains of gold of generations II and III; (**D**) thin gold veinlets of generation IV in grained aggregate of generation III; (**E**,**F**) zoned grain of gold of generations II and III with a gold rim of generation V and fine-grained aggregate of hypergenic, tenorite, and carbonate (Gip); (**F**) bornite inclusions (Bn) in gold of generation III.

We distinguish five generations of native gold [28]. Native gold of generation I occurs together with early paragenesis sulfides and forms 1–10 μm inclusions in magnetite, including that replacing the grains of Cr-spinel (Figure 5A,B). Its fineness varies in a wide range (580–960‰) even when gold particles are within a single cluster. It contains 0.4–1 wt % Pd and 0.1–1.3 wt % Cu (Table 3, Figure 3B).

Native gold of II–IV generations was deposited in the intergranular space of magnetite aggregates of late paragenesis. Gold grains attain 1–2 mm and are composed of polygrained aggregate of its various generations. Gold of generation II makes up the central parts of individual grains in such aggregates (Figure 5C) and is represented by Au–Ag–Cu–(Hg) solid solutions. Gold of this generation is characterized by considerable variations in the contents of Ag (2.8–26.7 wt %), Cu (6.6–24.2 wt %) and Hg (0–2.0 wt %) and rather stable fineness (648–744‰) (Table 2). Gold of generation III makes up the major volume of polygrained aggregates (Figure 5C,D). Its composition corresponds to Cu-bearing (to 2.9 wt % Cu) kustelite and electrum (fineness 280–514‰) or Au–Ag solid solution (fineness 810–853‰).

Gold of generation IV makes up a small part in the total mass of gold. It includes veinlet-like zones no more than 5–10 μm in thickness, developed in the intergranular space of polygrained gold aggregate (Figure 5D). The fineness of gold of generation IV is 740–853‰ and it contains Cu (1.4–3.8 wt %) and Hg (to 1.4 wt %) (Table 2).

Gold of generation V has the appearance typical of hypergenic gold. It replaces gold of earlier generations and has the highest fineness (933–976‰). Gold of generation V is also present in the fine-grained aggregate of minerals of hypergenic origin (iron hydroxides, tenorite, Cu–Mg carbonate, etc.) together with oxidized copper sulfides (Figure 5E,F). Its chemical composition corresponds to Au–Ag solid solution containing to 5 wt % Ag and 2.2 wt % Cu.

Table 3. Typical chemical composition and fineness of native gold of different generations from magnetite ores.

No. Sample/Grain	Generation	Au wt %	Ag wt %	Cu wt %	Hg wt %	Pd wt %	Total wt %	Fineness ‰
888/23	I	93.99	2.00	1.33	0.00	0.44	97.76	961
888/24		81.58	13.79	0.20	0.00	0.75	96.33	847
888/25		55.24	40.11	0.12	0.00	0.97	95.44	579
KAG-3/16	II	67.51	19.70	13.48	0.26	0.00	100.95	669
KAG-3/20		74.18	2.82	24.19	0.04	0.00	101.23	733
KAG-3/31		73.81	4.84	20.57	0.00	0.00	99.22	744
KAG-3/33		73.51	9.10	16.68	0.32	0.00	99.61	738
KAG-3/35		71.94	8.02	19.41	0.00	0.00	99.37	724
890b/42		64.86	26.70	6.58	2.00	0.00	100.14	648
KAG-3/5		65.82	20.36	11.91	0.00	0.00	98.09	671
890s/1	III	31.73	67.93	0.08	0.49	0.00	100.23	317
890s/6		28.22	72.28	0.56	0.00	0.00	101.06	279
890s/7		43.51	53.86	2.89	0.32	0.00	100.58	433
KAG-3/27		84.66	13.19	1.94	0.00	0.00	99.79	848
KAG-3/38		51.45	46.82	0.98	0.82	0.00	100.07	514
890/13		33.35	65.60	1.08	0.00	0.00	100.03	333
890s/9	IV	78.43	19.88	1.51	1.38	0.00	101.20	775
890s/4		74.11	22.35	2.31	1.43	0.00	100.20	740
890/7		84.88	10.85	3.79	0.00	0.00	99.52	853
890/14		74.09	24.26	1.38	0.00	0.00	99.73	743
KAG-3/29	V	95.60	2.99	0.45	0.00	0.00	99.04	965
KAG-3/45		96.46	0.20	2.21	0.00	0.00	98.87	976
KAG-3/47		92.24	4.99	1.62	0.00	0.00	98.85	933

Note. Microanalysis was performed in the IEM RAS (Institute of Experimental Mineralogy, Russian Academy of Sciences, Chernogolovka, Moscow Region, Russia), using electron scanning microscope CamScan MV2300 with energy-dispersive X-ray microanalyzer Link INCA Energy 300 (analyst D.A. Varlamov). Values of element concentration below 2σ (mean square error of analysis) are shown in italics. The reduced sum of elements in sample 888 is due to the small sizes of gold particles and partial entrapment of host magnetite (iron is excluded from the sum). The average measurement accuracy is 0.3 wt % for Au, Ag, Cu, Pd, and 1 wt % for Hg (which is associated with the possible migration of mercury from the analysis zone).

2.3. Physico-Chemical Conditions, Sources of Substance and Fluid and the Sequence of Formation of Gold Mineralization

Data on the research and estimation of P–T–X-parameters, sources of ore substance and fluid during the formation of gold mineralization veins at the Kagan ultramafic massif are reported in [7,9]. The isotopic composition of antigorite serpentinites is characterized by highly lightweight hydrogen -$\delta^{18}O$ = +5.2‰, δD = −127.7‰ [9]. This isotopic composition corresponds to continental serpentinites of lizardite–chrysotile type [29,30]. It is obvious that the studied antigorite serpentinites inherited the isotopic composition of earlier loop-shaped serpentinites. The lightweight isotopic composition of hydrogen includes talc from magnetite ores ($\delta^{18}O$ = +7.4‰, δ D = −132.7‰) and amphibole from amphibole–pyroxene ($\delta^{18}O$ = +9.3‰, δ D = −124.6‰) and pyroxene-amphibole rocks ($\delta^{18}O$ = +7.1‰, δ D = −126.2‰) from the Kagan massif. All these facts suggest a metamorphic origin of the fluid that takes part in the formation of gold mineralization. Such a fluid could result from the release of water (deserpentinization) during progressive metamorphism of early continental serpentinites and their replacement by olivine, enstatite, anthophyllite, and talc. Ultramafic rocks composed of these minerals are widespread at the Kagan massif, particularly in its southern part.

Study of the gas composition of fluid released during the thermal decrepitation (method gas chromatography) of primary inclusions at 300–600 °C in the minerals of antigorite serpentinite and magnetite ore showed that the composition of fluid has a X_{H2O} = 0.975–0.978 and fraction of carbon dioxide X_{CO2} = 0.019–0.020. To estimate the redox conditions of gold mineralization, we used the

indicator of the oxidation degree of volatiles $CO_2/(CO_2 + CO + H_2 + CH_4)$, which takes into account the ratio of oxidized and reduced gasses in the composition of inclusions [31]. This indicator was 0.84 during antigorization and 0.86 during the deposition of magnetite, which is the evidence that the gold mineralization of the studied types was formed under oxidizing conditions.

On the basis of available information on this object we propose the following scheme of the formation sequence of gold mineralization:

1. Upward movement of ultramafic rocks (harzburgites, dunites) to the surface, their serpentinization with the formation of early loop-shaped lizardites and/or chrysotile serpentinites with disseminated magnetite. Lizardite serpentinites at the Kagan massif only occur as small relics, whereas at the other ultramafic massifs of the Vishnevogorsk metamorphic complex (Nyashevskii, Ishkelskii, Borzovskii, etc.) they are widespread [14]. The presence of relicts of early loop-shaped serpentine (lizardite, chrysotile) in association with magnetite indicates that their formation temperatures were 100–300 °C.

2. Formation of the initial ore-forming fluid as a result of zonal metamorphism of early serpentinites and, probably, host rocks under the conditions of subgranulite-amphibolites facies (T = 60–700 °C and P = 5–10 kbar). Fluid is the result of release of water during deserpentinization of early serpentinites and transition of some ore components, such as Cu, Ag, Au, Zn, Mn, and S to solution.

3. Manifestation of fault tectonics within the massif and movement of the ore-bearing initial fluid along faults from the high-temperature zone to the lower-temperature zone of stability of antigorite and its discharge. In this zone the early loop-shaped serpentinite transforms into antigorite serpentinite with the growth of magnetite grains and formation of zoned magnetite rims on accessory Cr–spinel. Simultaneously, gold-ore mineralization of the first type is deposited along the thin cracks in schistose antigorite serpentinites. The formation of antigorite serpentinites took place under the upper degrees of green schist facies at the temperature of antigorite stability of 350–500 °C.

4. Continuation of the arrival of initial fluid into the open space of cracks and its mixing with meteoritic waters. The subsequent discharge of mixed fluid leads to the formation of the second type magnetite ores which carry sulfides and native gold of generation I of early paragenesis. Results of study of the composition of native gold with impurity of copper (II and III generations), combined with the diagram of the Au–Ag–Cu system [27], show that the temperature of gold deposition in magnetite ores could reach 350–450 °C (Figure 3B).

5. Cooling of the massif to conditions when antigorite becomes unstable and is replaced by chrysotile, chlorite, and talc. Recrystallization of rocks and gold-magnetite ores results in larger particles of copper sulfides and native gold of II–IV generations of late paragenesis. The temperature deposition conditions of minerals of late paragenesis were estimated using a chlorite geothermometer and were 310–210 °C [28].

6. In the conditions of hypergenesis zone, oxidation of copper and iron sulfides takes place with the formation of fine-grained aggregates of iron hydroxide (FeO(OH)), tenorite (CuO), Cu–Mg carbonate, and native gold of V generation.

3. Research Methods

3.1. Software and Thermodynamic Dataset for Modeling

Thermodynamic modeling of the first and second types of gold-ore mineralization was carried out using the Selektor-C software package (version 3.01, A.P. Vinogradov Institute of Geochemistry, Irkutsk, Russia), which implements the Gibbs energy minimization method based on the convex programming approach [32,33]. A detailed description of computational algorithms was given in [34]. The models used thermodynamic databases in the range of specified T–P parameters: for minerals [35–42], gases [43], and components of aqueous solution [44–52].

This method was widely used in the modeling of the formation of native gold: hypogene and hypergene models of the Kyuchyus Au–Sb–Hg deposit (Yakutia, Russia), including mercuric gold [53]; models of quaternary solid solutions in hydrothermal conditions at the Aitik Au–Ag–Cu porphyry

deposit (Sweden) and the hydrothermal-hypergene model of formation of Au–Cu intermetallics at the Wheaton Creek placer deposit (Canada) [54]; the model of the Au–Ag, Ag–Pb, and Ag–Au–Pb mineralization at the Rogovik epithermal gold–silver deposit in the Omsukchan ore district (northeastern Russia) [55].

In the study we used the method of multi-reservoir dynamics, which involves separation of the complex system into a series of individual subsystems–reservoirs. The initial aqueous solution subsequently interacts with the rock in the first reservoir at temperature T_1 and pressure P_1, altered solution passes to the second reservoir and interacts with the rock at T_2 and P_2 etc. Thus, the alternating aqueous solution passing through a series of reservoirs changes the rock composition in the reservoirs. The introduction of the mode of successive passing of a certain amount of portions of the solution allows us to form an equilibrium-dynamic model which can be used for studying the processes of formation and alteration of ore mineralization. A similar approach was earlier used by us for modeling the formation of magnetite–chlorite–carbonate rocks with copper-bearing gold–silver solid solution at the Karabash ultramafic massif [11].

Modeling was completed for the K–Mg–Mn–Ca–Al–Si–Ti–Fe–Cu–Ag–Au–Cr–Hg–S–Cl–C–H–O system. The thermodynamic properties of minerals, binary, ternary and quaternary solid solutions, aqueous, and gaseous species considered in the models were the same as in [11] (Tables S2 and S3 of the Supplementary Materials from [11]). Thermodynamic constants for chlorites, ilmenites, pyroxenes, carbonates, olivines, and plagioclases, which are natural binary and ternary solid solutions, as well as solid solutions of quaternary system Ag–Au–Cu–Hg, were calculated considering the activity coefficients of end members for the accepted models of solid solutions [33,35,54,56]. Serpentinite was introduced as an ideal solid solution consisting of antigorite and lizardite. Cr–spinel is represented by an ideal model of solid solution $FeCr_2O_4$–$MgAl_2O_4$–$MgFe_2O_4$–$MgCr_2O_4$ [57].

3.2. Initial Data for Thermodynamic Modeling

The formation of the gold-ore mineralization begins with the generation of initial metamorphic ore-forming fluid as a result of the high-temperature zonal metamorphism of early serpentinites. The composition of these serpentinites was specified from the average composition of 19 samples of serpophite–lizardite serpentinites of the Vishnevogorsk–Ilmenogorsk metamorphic complex (Table 4).

Table 4. The composition of serpophite–lizardite (1) and antigorite (2) serpentinites (in wt %).

Components	1 *	2 **
SiO_2	38.93	39.0
TiO_2	0.01	0.025
Al_2O_3	1.39	1.49
Cr_2O_3	0.38	0.197
Fe_2O_3	5.33	5.90
FeO	2.2	2.4
MnO	0.07	0.07
MgO	36.98	38.0
CaO	0.82	0.04
K_2O	-	0.01
H_2O	1.15	-
LOI	13.23	12.5
CO_2	1.15	-
CuO	-	0.03
S	-	0.02
Au (ppm)		0.010
Ag (ppm)		0.888

* data from [14]; ** we used the data of X-ray spectral fluorescent (CPM-35 and XRF 1800), chemical (FeO, CuO, S), ICP-MS (Ag) and chemical spectral (Au) analyses conducted in the CKP Geoanalysist in the Institute of Geology and Geochemistry, UrB RAS (analysists N.P. Gorbunova, L.A. Tatarinova, G.S. Neupokoeva, I.I. Neustroeva, and G.A. Avvakumova).

The calculation of the composition of initial metamorphic fluid was performed for T = 700 °C, P = 10 kbar. In these P–T conditions early serpentinites transform into rocks composed of mainly olivine and enstatite. The calculated composition of the metamorphic water fluid separated during dehydration is given in Table 5. This composition was used in further calculations in the 14-reservoir model. All 14 reservoirs of the model are represented by antigorite serpentinite. The chemical composition of a typical sample of antigorite serpentinite, containing gold mineralization, used in the calculations, is reported in (Table 4). Amount of volatiles: HCl = 0.01 mole.

Table 5. Calculated composition of initial metamorphic fluid at 700 °C and 10 kbar.

Components	Composition, mol/kg H_2O
C	1.811
Mg	3.980×10^{-3}
Mn	6.682×10^{-2}
Al	6.552×10^{-8}
Si	1.947×10^{-1}
S	4.323×10^{-2}
Cl	6.932×10^{-1}
Ca	2.404×10^{-1}
Fe	3.326×10^{-2}
Cu	7.608×10^{-3}
Ag	5.705×10^{-5}
Au	3.519×10^{-7}
Cr	6.904×10^{-10}
H	4.199×10^{-1}
O	4.092
pH	4.357
$\log f_{O2}$	–15.05
$\log f_{S2}$	0.829

3.3. Scenarios of Thermodynamic Modeling

We have modeled two scenarios of formation of gold-ore mineralization: metasomatic interaction of metamorphic fluid with serpentinites (scenario 1) and mixing of two fluids: ascending metamorphic and descending meteoric and their discharge in the free space of cracks of schistose serpentinites (scenario 2).

In the calculations under scenario 1, we obtained interaction products of 20 portions of deep-seated metamorphic fluid flowing consistently through nine serpentinite reservoirs at total drop of T from 650 to 250 °C and P from 4.5 to 0.5 kbar (Figure 6). From one reservoir to another, temperature drops by 50 °C and pressure by 0.5 kbar. The simulation was carried out at the rock/water ratio (R/W) = 10. The weight of a portion of metamorphic fluid is 100 g, the weight of each reservoir is 1 kg of serpentinites.

The model for scenario 2 involves two flows: ascending deep-seated metamorphic and descending, resulting from the interaction of meteoric waters with antigorite serpentinites at corresponding temperatures and pressures (Figure 6).

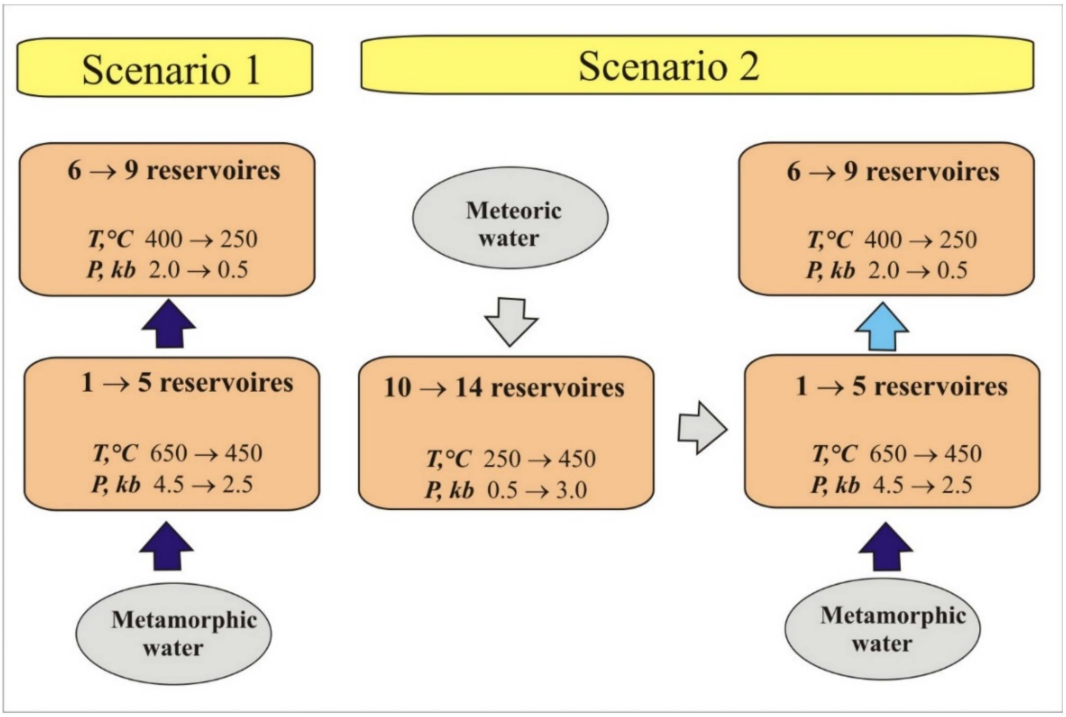

Figure 6. Scheme for calculation of 14-reservoir model in scenarios of metasomatic interaction of metamorphic fluid with serpentinite (Scenario 1) and mixing of metamorphic and meteoric fluids (Scenario 2).

The initial data of the model: 100 g of metamorphic fluid, 1 kg of meteoric water, weights of serpentinites are 100 g (reservoirs 1, 2, 8–14) and 5 g (reservoirs 3–7). The increase in the amount of rocks in reservoirs 3–7 is related to the imitation of fluid interaction with the walls of the open crack or weakened zone.

The P, T parameters for two models given in Table 6.

Table 6. T, P parameters of reservoirs.

Reservoir	T, °C	P, kbar
1	650	4.5
2	600	4
3	550	3.5
4	500	3
5	450	2.5
6	400	2
7	350	1.5
8	300	1
9	250	0.5
10	250	0.5
11	300	1
12	350	1.5
13	400	2
14	450	3

4. Results of Thermodynamic Modeling

Scenario of metasomatic interaction of metamorphic fluid with serpentinites simulated the formation of the first type gold-ore mineralization in schistose serpentinites. Figures 7 and 8 show the calculation results after passing of 20 portions of fluid in the flow regime reactor at R/W = 10.

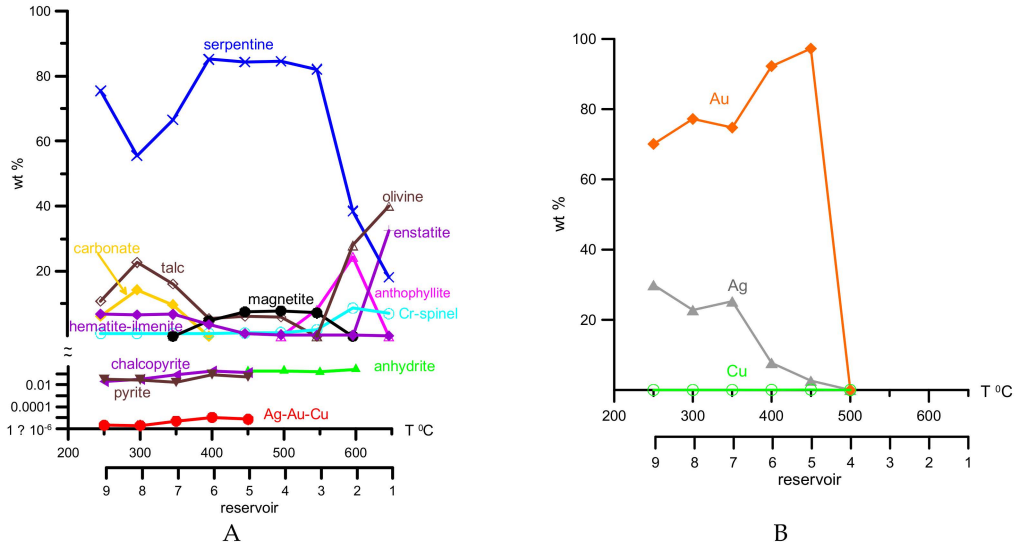

Figure 7. Mineral composition of reservoirs after passing of 20 portions of metamorphic fluid (**A**) and composition of Ag–Au–Cu solid solutions (**B**) in the model under scenario 1.

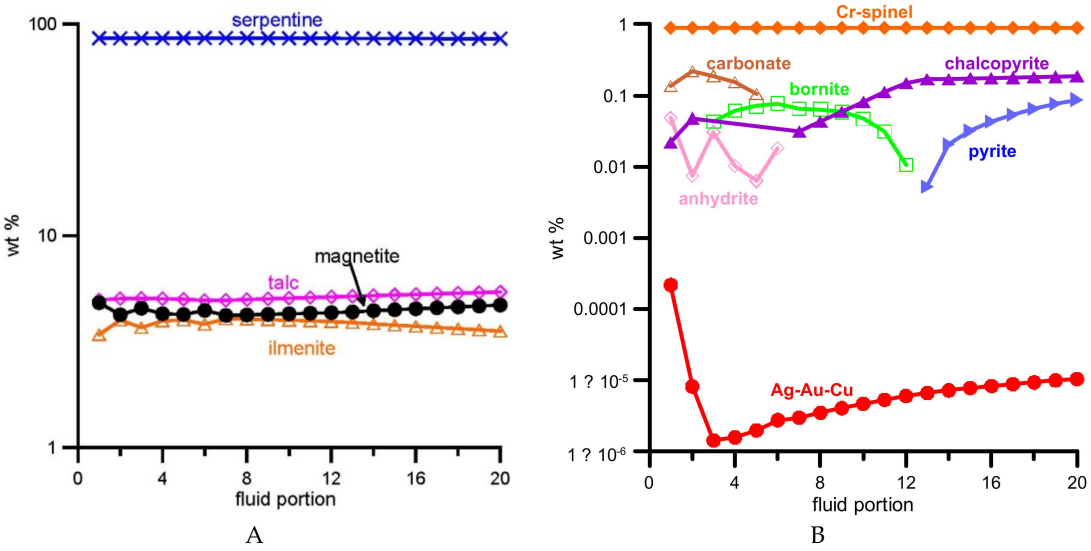

Figure 8. Mineral composition of reservoir 6 (T = 400 °C, P = 2 kbar). (**A**) major minerals; (**B**) minor minerals.

At T below 550 °C, olivine–enstatite rock transforms into serpentinites with a small amount of talc and magnetite, and below 400 °C, carbonate appears in serpentinite and the content of talc increases (Figure 7A). The content of accessory minerals in serpentinites is no more than 1 wt %. Among them, at T above 400 °C, anhydrite is formed and at lower temperature, chalcopyrite and pyrite.

In the range of 450–250 °C (reservoirs 5–9) the solid solution Ag–Au–Cu (<0.1 wt % Cu) is deposited. Its fineness varies depending on temperature conditions in the reservoirs and has a tendency to decrease from 950‰ at 450 °C to 700‰ at 250 °C, which corresponds the content of Ag from 0 to 30 wt % (Figure 7B).

A minor amount of gold (to 0.1 ppm) is formed in reservoir 6 at T = 400 °C. The supply of the first portions of fluid does not influence the content of rock-forming minerals (serpentine, talc, magnetite, ilmenite) in this reservoir (Figure 8A). At the same time, secondary carbonate and anhydrite, deposited with the first portions of fluid, with the arrival of additional portions are replaced by bornite and thereafter by chalcopyrite and pyrite (Figure 8B). Further arrival of new portions of fluid increases the content of the Ag–Au–Cu solid solution to 0.1 ppm.

Modeling for the scenario on discharge of metamorphic and meteoric fluids in the open space of cracks reflects the formation of gold-ore mineralization of the second-type in veined magnetite ores. The model involves mixing and further discharge of two types of fluids, metamorphic and surface meteoric, in the open space of cracks. Metamorphic fluid is formed during deserpentinization of lizardite–chrysotile serpentinites, and its initial composition is similar to the fluid from scenario 1. The fluid of meteoric origin is formed during the interaction of submerging meteoric waters [53] with antigorite serpentinites. Oxygen of meteoric fluid is a strong exogenous oxidizer of deep-seated iron in the formation of magnetite ores [58].

Results of the mineral composition modeling for altered serpentinites after passing of 20 portions of fluid through a sequence of reservoirs in the flow reactor regime are given in Figures 9 and 10.

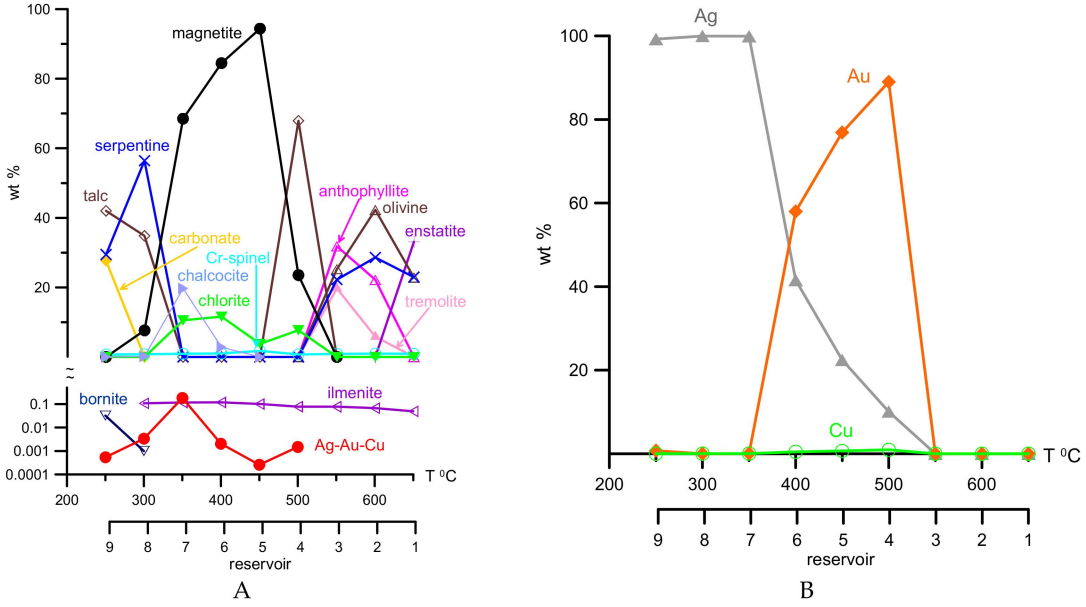

Figure 9. Results of the ascending branch of the model in scenario 2. (**A**) mineral composition of reservoirs; (**B**) composition of Ag–Au–Cu solid solutions.

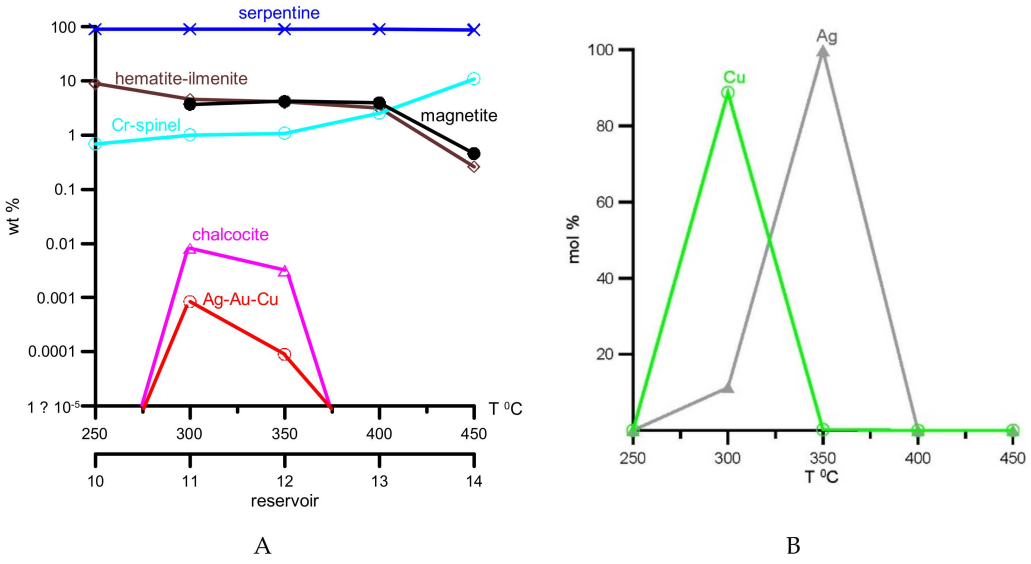

Figure 10. Results of descending branch of the model in scenario 2. (**A**) mineral composition of reservoirs; (**B**) composition of Ag–Au–Cu solid solutions.

The high temperature reservoirs (1–3) of the ascending branch of the model are represented by olivine–enstatite rocks containing serpentine (Figure 9A). When the temperature decreases from 700 to 550 °C, olivine and enstatite are replaced by anthophyllite and tremolite. Further decrease in temperature leads to the formation of magnetite together with talc and chlorite (500 °C), and at 350–450 °C magnetite becomes the main mineral with minor chlorite, chalcocite, and Cr–spinel. In the range of 500–250 °C, Ag–Au solid solution also forms and its maximum content in the rock amounts to 0.1 wt % at 350 °C. In this solid solution gold dominates over silver at 400–500 °C, and with decreasing temperature, gold content reduces and becomes mainly silver (Figure 9B). At temperatures below 350 °C, one can observe a mineral association of serpentine with talc, to which at 250 °C carbonate is added.

Mineral composition of rocks of the descending branch of the model (reservoirs 10–14) is represented by serpentinites and small amounts (less than 10 wt %) of Cr–spinel, magnetite and hematite–ilmenite (Figure 10A). At 350–300 °C, accessory chalcocite is present in the rock. In the descending branch of the model Au is absent in the composition of solid solutions. Here they contain only Ag (reservoir 12) and Cu (reservoir 11) (Figure 10B).

In scenario 1, imitating the influence of metamorphic deep-seated fluid on serpentinites, the solution equilibrated with rocks becomes more acidic (pH decreases) with the arrival of the new portions of fluid. After the arrival of 10 portions, pH of the solution attains the steady state. In this state the minimum value of pH = 4 is attained at 450 °C. When the temperature increases to 650 °C or decreases to 250 °C, pH of the solution equals 4.5 (Figure 11A).

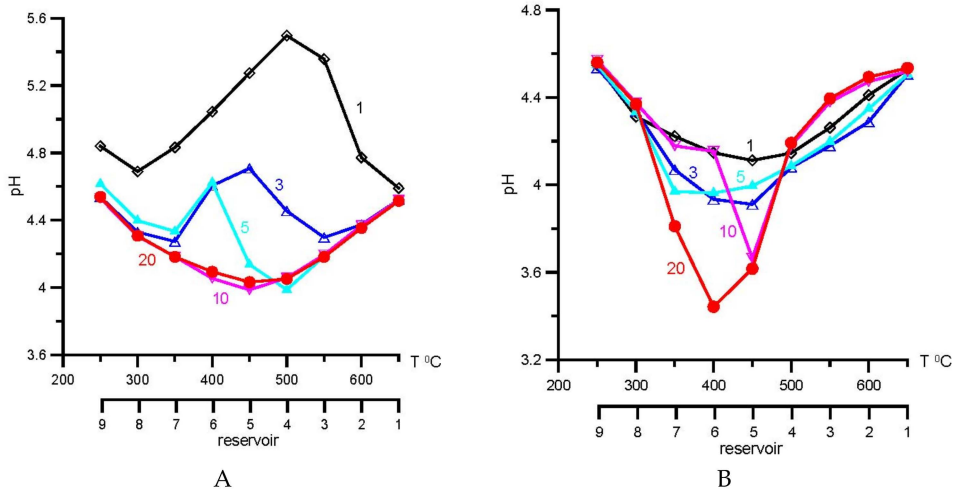

Figure 11. Change in pH of reservoirs after the arrival of various amounts of portions of fluid. (**A**) scenario 1; (**B**) scenario 2.

In scenario 2 the behavior of pH in general shows the same tendency as in scenario 1, but here the contribution of the oxidative meteoric fluid supplied to reservoir 5 plays a significant part. The system attains a stationary state after the arrival of more than 20 portions of the solution and minimum value of pH = 3.4 at 400 °C (Figure 11B).

Fugacity values of oxygen and sulfur in both scenarios of modeling have a tendency to reduce with decreasing temperature in the reservoirs (from reservoir 1 to 9) (Figure 12).

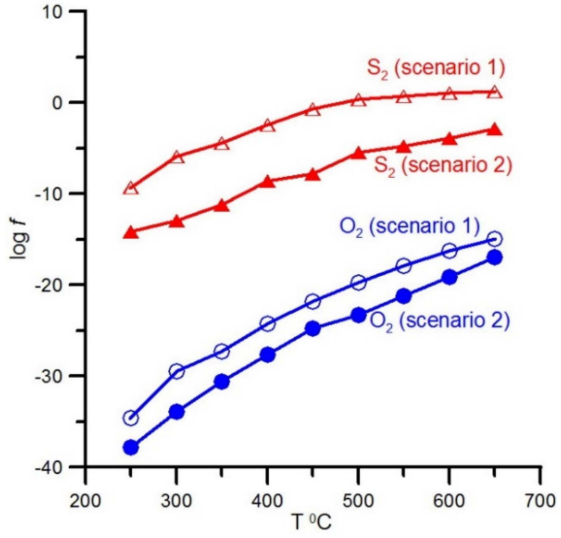

Figure 12. Changes in fugacities of oxygen and sulfur in scenarios 1 and 2 after the arrival of 20 portions of fluid.

In reservoirs with T > 450 °C, the fluid is dominated by the chloride complex of gold $AuCl_2^-$ [59] (Figure 13). As the temperature decreases, the dominant role of chloride complex is replaced by hydrosulfide $AuHS^0$ (scenario 1) or hydroxide $AuOH^0$ complexes (scenario 2) [60]. The predominance of gold hydroxide in scenario 2 is related to a more oxidized state of fluid owing to the arrival of meteoric waters.

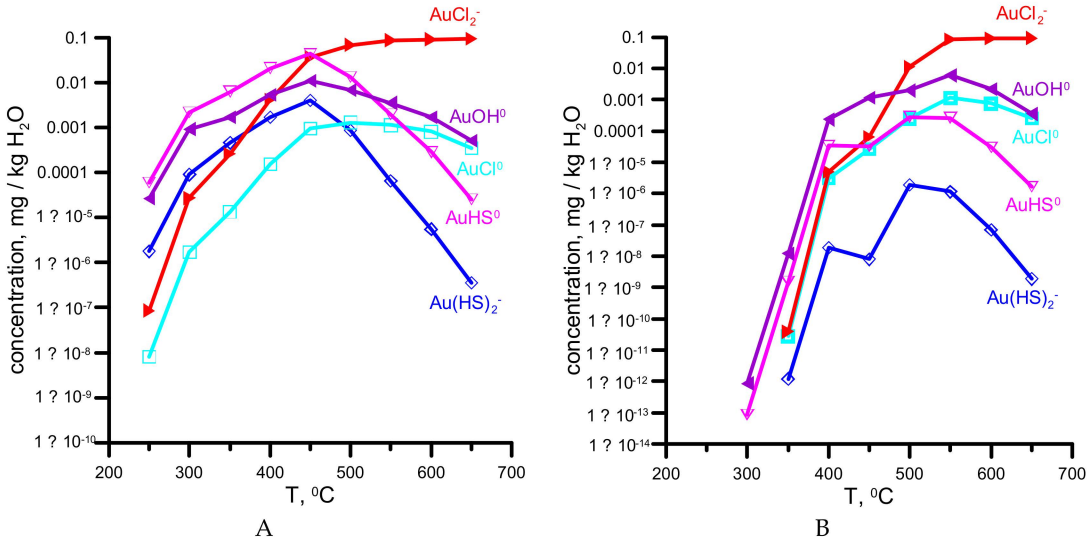

Figure 13. Forms of Au transfer in scenarios 1 (**A**) and 2 (**B**).

The content of gold deposited in the rocks under scenarios 1 and 2 differs considerably. In scenario 1 the amount of gold in serpentinites is no more than 0.1 ppm, whereas in scenario 2 its content in magnetite ore amounts to 10–13 ppm (Figure 14A). At the same time, the maximum gold contents in both scenarios are achieved at T = 400 °C (reservoir 6). Consistent accumulation of gold in reservoir 6 with the arrival of new portions of fluid is shown in Figure 14B.

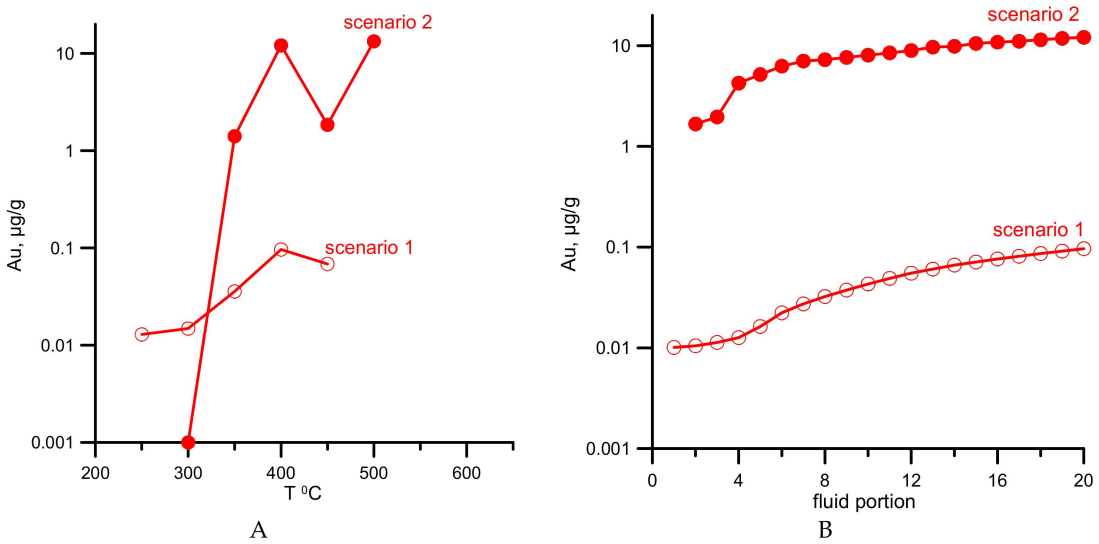

Figure 14. The amount of gold in scenarios 1 and 2. (**A**) after the arrival of 20 portions of fluid at different temperatures in reservoirs; (**B**) with the arrival of new portions of fluid in reservoir 6 (400 °C and 2 kbar).

5. Discussion

5.1. Comparative Analysis of Agreement of Model and Natural Mineral Associations

Our calculations of the formation of gold-ore mineralization can explain some questions that arise when studying serpentinite massifs of ultramafic rocks, including the object of the present study. In particular, calculations for scenario 1 contribute to the solution of the earlier stated problem [61] about the discrepancy of the scales of primary and placer gold content in the areas where ultramafic rocks are spread. Although the placers of streams draining ultramafic massif are of commercial value, findings of native gold in serpentinites are scarce [62–64]. The above-given calculations for scenario 1 show that, in the model of formation of gold mineralization from cooling metamorphic fluid, gold is concentrated from relatively low concentrations of no more than 0.1 ppm (Figure 14). Nevertheless, the washout of extended zones of schistose antigorite serpentinites by streams can lead to the formation of placers with considerable reserves.

Comparative analysis of mineral associations in the first type gold mineralization at the Kagan massif and those obtained in scenario 1 (Table 7) indicates similarities in the low gold content in rocks (to 0.1 ppm).

Moreover, the rocks contain small amounts of magnetite and talc which replaces serpentine. The fineness of Au–Ag solid solutions in calculated and natural associations is no more than 750‰ and they have similar deposition temperatures (300–500 °C). At the same time, accessory chalcopyrite and pyrite occur in paragenesis with Au–Ag solid solutions in scenario 1, but these sulfides were absent in natural samples. Most likely, this difference is due to the very low content of sulfides in antigorite serpentinites of the Kagan massif.

Rocks with a high magnetite content within the model of cooling metamorphic fluid (scenario 1) in the processes of its metasomatic interaction with host serpentinites or discharge in the open space of cracks in the whole range of temperatures and pressures have not been obtained. The mineral association of magnetite, the content of which drastically prevails over serpentine, talc, amphibole and chlorite, was obtained only by strong dilution of metamorphic fluid with weakly mineralized waters in scenario 2. The diluting fluid in this scenario is meteoric water seeping through the bed of serpentinites to the depth.

Table 7. Comparative characteristics of minerals and mineral associations of gold mineralization from Kagan massif and model calculations for scenarios 1 and 2.

Characteristics	Kagan Massif		Calculated Data	
	1 Type of Gold Mineralization	2 Type of Gold Mineralization	Scenario 1	Scenario 2
Quantitative ratios of main minerals *	Atg > Ctl, Tc > Chl > Tr, Mag	Mag >> Atg > Tc > Tr, Chl, Ctl, Dol	Srp >> Tc, Mag > Ilm–Hem	Mag >> Srp > Tc > Tr, Chl
Quantitative ratios of accessory minerals	Pn > Au(ss)	Ccp > Po, Pn > Cub, Bn, Tal, Sp > Au(ss)	Ccp, Py >> Au(ss)	Ilm–Hem > Cct > Bn, Au(ss)
Sequence of mineral deposition **	Atg, Tr, Mag, Pn, Au(ss) → Tc, Chl, Ctl	Mag, Atg, Ccp, Po, Cub, Tal, Pn, Au(ss) → Tr, Tc, Ctl → Ccp, Bn, Po, Sp, Au(ss) → Chl, Srp, Dol	Srp, Mag, Tc, Ccp, Py, Au(ss) → Srp, Tc, Cb, Ilm–Hem, Au(ss)	Ol, Srp, Ath, Tr → Mag, Chl, Tc, Ilm–Hem, Au(ss) → Mag, Chl, Cct, Au(ss) → Srp, Tc, Cb, Bn, Au(ss)
T °C of gold deposition	500–300		450–250	500–350
Composition of solid solutions gold/fineness ‰	ss(Au,Ag)/772–996	ss(Au,Ag)/580–960, ss (Au,Ag,Cu)/648–744 ss (Au,Ag,Cu)/280–853	ss(Au,Ag)/900–950 ss(Au,Ag)/700–800	ss(Au,Ag)/600–900 ss(Au,Ag)/600 ss(Ag,Au)/0–600
Gold content in rock/ore, ppm	To 0.1	0.2–1.2 and more	To 0.1	To 10

* For calculated data at P, T of gold deposition; ** for calculated data from high- to low-temperature reservoir. Ath—anthophyllite; At—gantigorite; Au(ss)—Au–Ag–Cu solid solution; Bn—bornite; Cb—carbonate; Ccp—chalcopyrite; Cct—chalcocite; Chl—chlorite; Ctl—chrysotile; Cub—cubanite; Dol—dolomite; Ilm–Hem—ilmenite–hematite; Mag—magnetite; Ol—olivine; Pn—pentlandite; Po—pyrrhotite; Py—pyrite; Sp—sphalerite; Srp—serpentine; Tal—talnakhite; Tc—talc; Tr—tremolite.

Comparative analysis of mineral associations in the second type of gold mineralization and those obtained in scenario 2 showed both a good similarity of natural and calculated ratios of main and accessory minerals of rocks and identical sequence of their deposition in the open space of cracks (see Table 5). The contents of gold in the model calculations in scenario 2 attain 10–13 ppm and correspond to their level in magnetite ores from the Kagan massif. Calculations for this scenario support the probability of formation of several generations of Au–Ag solutions, covering the whole range of compositions from pure gold to pure silver. However, in the calculations we did not obtain Au–Ag solid solutions with elevated copper content typical of native gold of generation II in magnetite ores.

5.2. The Possible Sources of Gold, Silver, and Other Metals

Previous studies of the massifs of ultramafic rocks revealed spatial overlapping of many placers of the Urals with antigorite serpentinites as well as considerable redistribution and concentration of gold during antigoritization [6,7,9]. On the basis of these facts a conclusion was made about the origin of gold-ore mineralization in the crustal period of the history of the formation of ultramafic massifs during regional and local metamorphism, and the gold-productive serpentinite (antigorite) metasomatic formation was also distinguished [7].

Magnetite ores in ultramafic rocks in world literature were described in [65–69]. They are suggested to be of different genesis—magmatic [67], metamorphic [65,69], and hydrothermal [68].

Rare cases of elevated gold contents in magnetite ores are known [70,71]. In the Bou–Azzer mantle ophiolite complex (Anti-Atlas, Morocco), strongly serpentinized periodite is known to contain magnetite veins formed by filling the open space of cracks [71]. Magnetite in the veins is associated with serpentine, magnesite, clinochlore, talc, and andradite. The relatively minor enrichment of magnetite in gold (to 8–14 mg/t) is attributed to the hydrothermal process, and the high mobility of iron is explained by the high water/rock ratio during serpentinization [71].

Magnetite ores in ultramafic rocks enriched with Au and Ag (a few tens of ppb) are widely spread within the massifs of West Mongolia [70]. Veins of massive magnetite ores up to 10 cm thick syngenetic to the processes of serpentinization occur there. Gold and silver are considered to be brought by serpentinized solutions borrowing these elements from chromitites or volcano–sedimentary rocks.

In this work we propose hydrothermal–metasomatic models of the formation of gold mineralization in which deserpentinizing early lizardite-chrysotile serpentinites are the source of metal and water. Metals and water are separated from early serpentinites during high-temperature metamorphism, and the metamorphic fluid moves to the lower temperature discharge region along the schistosity zones in the massif of ultramafic rocks. Metasomatic interaction of the metamorphic fluid with serpentinites in the discharge zones can result in poor gold-ore mineralization in the form of native gold disseminated in schistose serpentinites. A necessary condition for the formation of hydrothermal rich gold-ore mineralization in magnetite veins is mixing of metamorphic and meteoric fluid at T = 500–400 °C and P = 2–3 kbar and discharge of deep-seated and meteoric fluids in the open space of cracks. The mechanism of mixing of the deep-seated and meteoric fluids was used earlier in modeling of the formation of Au–REE mineralization in magnetite–chlorite–carbonate rocks from the Karabash ultramafic massif [11].

5.3. Sulfur Fugacity Evolution During Gold-Ore Mineralization Formation in Ultramafic Rocks and Magnetite Ores

The composition of Au–Ag solid solutions deposited under both scenarios at 500–300 °C depends on sulfur fugacity (fS_2) in the specified range of temperatures. In the model under scenario 1, Au–Ag solid solutions form in the field of high and very high values of fS_2 and are arranged along the covellite (Cv)–digenite (Dg) equilibrium line (Figure 15). The molar fraction of silver in Au–Ag alloys (X_{Ag}) in this model, according to experimental data [72], is less than 0.2 (12 wt % Ag). This composition agrees well with that of native gold in schistose serpentinites from the Kagan massif (see Table 2 and Figure 3A).

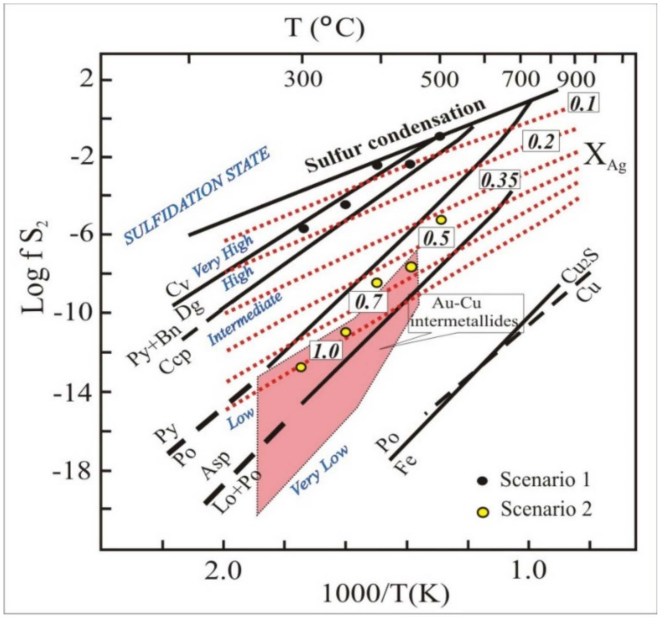

Figure 15. Sulfur fugacity versus temperature diagram (modified from [72]) showing the formation conditions of Au–Ag solid solutions at 300–500 °C in Scenarios 1 and 2. Dotted lines show sulfidation of silver in Au–Ag melts with a varying molar fraction of Ag (X_{Ag}) from data [73]. Field of Au–Cu intermetallids in rodingites from Zolotaya Gora deposit of Southern Urals is shown [12].

In the model for scenario 2, Au–Ag solid solutions are formed in the field of low values of fS_2 below the pyrrhotite–pyrite on the T–log fS_2 diagram (see Figure 15). The formation conditions of these solid solutions partially coincide with those of Au–Cu intermetallides from rodingites at the Karabash massif in the Southern Urals [12]. The composition of Au–Ag solid solutions in scenario 2 is

$X_{Ag} > 0.4$ (26.7 wt % Ag) and is in general similar to that of native gold from magnetite ores of the Kagan massif (see Table 3 and Figure 3B).

6. Conclusions

1. We have constructed thermodynamic models of the formation of two types of gold-ore mineralization at the Kagan ultramafic massif in the Southern Urals. Metamorphic water which results from dehydration of early serpentinites during high-temperature zonal regional metamorphism (700 °C, 10 kbar) is considered the source of ore-bearing fluid. This water extracts metals from rocks in the high-temperature zones and moves along the faults to the lower temperature region. Metasomatic interaction of the metamorphic fluid with serpentinites in the transit zone in scenario 1 is responsible for the formation at T = 450–250 °C and P = 2.5–0.5 kbar of gold-poor mineralization (to 0.1 ppm) of type 1 disseminated in schistose rocks. A necessary condition for the formation of hydrothermal gold-rich mineralization (to 10–13 ppm and more) in magnetite veins of type 2 in scenario 2 is mixing of metamorphic and meteoric fluid at T = 500–400 °C and P = 2–3 kbar and discharge of mixed fluid in the open space of cracks in schistose serpentinites.

2. The mineral associations, quantitative ratios, and sequence of deposition of the main minerals and composition of Au–Ag solid solutions obtained in scenarios 1 and 2 are, on the whole, similar to the natural types of gold mineralization at the Kagan massif. In mineralization of type 1, serpentinite contains small amounts of magnetite and talc which replaces antigorite that prevails over chrysotile and lizardite. Calculated and natural associations are characterized by Au–Ag solid solutions with the fineness higher than 750‰ and close deposition temperatures (300–500 °C). In type 2, association of magnetite occurs, which drastically dominates over serpentine, talc, amphibole, and chlorite. In this association several generations Au–Ag solid solutions are formed, which cover the whole range of compositions from virtually pure gold to pure silver.

3. The model calculations show that at temperatures higher than 450 °C the fluid with pH = 3.5–4.5 is dominated by the gold chloride complex $AuCl_2^-$, and with decreasing temperature the dominant role of chloride complex is replaced by hydrosulfide $AuHS^0$ (scenario 1) or hydroxide $AuOH^0$ (scenario 2). The predominance of gold hydroxide in scenario 2 is related to a more oxidized state of fluid owing to the arrival of meteoric waters.

4. The composition of Au–Ag solid solutions deposited in both scenarios at 500–300 °C is determined by the value of sulfur fugacity (fS_2). In the model for scenario 1, Au–Ag solid solutions are formed at high fS_2 values ($10^{-0.4}$–10^{-6}) that correspond to the lines of buffer reaction covellite–digenite, and in scenario 2, at low values of fS_2 ($10^{-5.5}$–10^{-14}) below the buffer line pyrrhotite–pyrite on the T–fS_2 diagram.

Author Contributions: Conceptualization, V.M., K.C., and G.P.; Methodology, V.M., K.C., and G.P.; Software, K.C.; Investigation, D.V.; Data Curation, V.M., K.C., and G.P.; Writing-Review & Editing, G.P.; Visualization, V.M. and K.C.; Supervision, G.P.

Funding: This work was supported by the Russian Foundation for Basic Research (grant 16-05-00407a) and state assignments of IGM SB RAS, IG SB RAS, IGG UB RAS (No AAAA-A18-118052590028-9), IEM RAS (No AAAA-A18-118020590151-3) financed by Ministry of Science and Higher Education of the Russian Federation.

Acknowledgments: Our thanks go to Velivetskaya, T.A., and Shanina, S.N., Gorbunova N.P., Tatarinova L.A., and Neupokoeva G.S. for the analytical data. We thank the Reviewers for the important comments and constructive suggestions, which helped us to improve the quality of the manuscript.

Conflicts of Interest: The authors declare no conflict of interest.

References

1. Benevolsky, B.I. *Gold of Russia. Problems of the Use and Reproduction of the Mineral Resource Base*; Geoinformmark: Moscow, Russia, 1995; 87p. (In Russian)
2. Sazonov, V.N.; Ogorodnikov, V.N.; Koroteev, V.A.; Polenov, I.A. *Gold Deposits of the Urals*, 2nd ed.; Ural Mining and Geological Academy: Yekaterinburg, Russia, 2001; 622p. (In Russian)

3. Ovchinnikov, L.N. *Minerals and Metallogeny of the Urals*; Geoinformmark: Moscow, Russia, 1998; 412p. (In Russian)
4. Puchkov, V.N. General features relating to the occurrence of mineral deposits in the Urals: What, where, when and why. *Ore Geol. Rev.* **2017**, *85*, 4–29. [CrossRef]
5. Borodaevsky, N.I. Types of gold deposits related to ultramafic rocks in the Miass and Uchaly districts in the southern Urals. In *200 Years of Gold Industry of the Urals*; Ivanov, A.A., Rozhkov, I.S., Eds.; UFAN SSSR: Sverdlovsk, Russia, 1948; pp. 316–330. (In Russian)
6. Berzon, R.O. *Gold Resource Potential of Ultramafics*; VIEMS: Moscow, Russia, 1983; p. 47. (In Russian)
7. Sazonov, V.N. *Gold-Productive Metasomatic Rocks in Mobile Belts: Geodynamic Settings and PTX Parameters of Their Formation and Implications for Forecasting*; Ural Mining and Geological Academy: Yekaterinburg, Russia, 1998; 181p. (In Russian)
8. Spiridonov, E.M.; Pletnev, P.A. *Zolotaya Gora Deposit of Cupriferous Gold*; Nauchnyi Mir: Moscow, Russia, 2002; 220p. (In Russian)
9. Murzin, V.V.; Varlamov, D.A.; Shanina, S.N. New Data on the Gold–Antigorite Association of the Urals. *Dokl. Earth Sci.* **2007**, *417*, 1436–1439. [CrossRef]
10. Murzin, V.V.; Varlamov, D.A.; Ronkin, Y.L.; Shanina, S.N. Origin of Au-bearing Rodingite in the Karabash Massif of Alpine-Type Ultramafic Rocks in the Southern Urals. *Geol. Ore Depos.* **2013**, *55*, 278–297. [CrossRef]
11. Murzin, V.; Chudnenko, K.; Palyanova, G.; Kissin, A.; Varlamov, D. Physicochemical model of formation of gold-bearing magnetite–chlorite–carbonate rocks at the Karabash ultramafic massif (Southern Urals, Russia). *Minerals* **2018**, *8*, 306. [CrossRef]
12. Murzin, V.V.; Chudnenko, K.V.; Palyanova, G.A.; Varlamov, D.A.; Naumov, E.A.; Pirajno, F. Physicochemical model of formation of Cu–Ag–Au–Hg solid solutions and intermetallic alloys in the rodingites of the Zolotaya Gora gold deposit (Urals, Russia). *Ore Geol. Rev.* **2018**, *93*, 81–97. [CrossRef]
13. Bazhin, E.A. *Gold Content of the Talovskii Gabbro-Ultramafic Massif (Southern Urals). Problems of Mineralogy, Petrography and Metallogeny; Scientific Readings in Memory of P.N.Chirvinskii: Collection of Scientific Articles*; Issue 15; Perm State Research University: Perm, Russia, 2012; pp. 294–298. (In Russian)
14. Varlakov, A.S.; Kuznetsov, G.P.; Korablev, G.G.; Murkin, V.P. *The Ultrabasites of Vishnyevogorsk-Ilmenogorsk Metamorphic Complex (South Urals)*; Edition of Institute of Mineralogy Ural Division of Russian Academy of Sciences: Miass, Russia, 1998; 195p. (In Russian)
15. Murzin, V.V. Oxygen and Hydrogen Isotopic Composition of the Fluid during Formation of Anthophyllite Metaultramafic Rocks in the Sysert Metamorphic Complex, Central Urals. *Dokl. Earth Sci.* **2014**, *459*, 1548–1552. [CrossRef]
16. Murzin, V.V.; Hiller, V.V.; Varlamov, D.A. The age position of gold–sulfide mineralization in the metahyperbasites of the Sysert' metamorphic complex in the Middle Urals. *Litosfera* **2015**, *4*, 87–92. (In Russian)
17. Reith, F.; Brugger, J.; Zammit, C.M.; Nies, D.H.; Southam, G. Geobiological cycling of gold: From fundamental process understanding to exploration solutions. *Minerals* **2013**, *3*, 367–394. [CrossRef]
18. Kerr, G.; Craw, D. Mineralogy and geochemistry of biologically-mediated gold mobilisation and redeposition in a semiarid climate, Southern New Zealand. *Minerals* **2017**, *7*, 147. [CrossRef]
19. Kalinin, Y.A.; Palyanova, G.A.; Naumov, E.A.; Kovalev, K.R.; Pirajno, F. Supergene remobilization of Au in Au-bearing regolith related to orogenic deposits: A case study from Kazakhstan. *Ore Geol. Rev.* **2019**, *109*, 358–369. [CrossRef]
20. Kalinin, Y.A.; Palyanova, G.A.; Bortnikov, N.S.; Naumov, E.A.; Kovalev, K.R. Aggregation and Differentiation of Gold and Silver during the Formation of the Gold-Bearing Weathering Crusts (on the Example of Kazakhstan Deposits). *Dokl. Earth Sci.* **2018**, *482*, 1193–1198. [CrossRef]
21. Saunders, J.A.; Burke, M. Formation and aggregation of gold (electrum) nanoparticles in epithermal ores. *Minerals* **2017**, *7*, 163. [CrossRef]
22. Murzin, V.V.; Varlamov, D.A. Noble metals in magnetite ores of the Kagan ultramafic massif in the Southern Urals. In *Yearbook-2005/Institute of Geology and Geochemistry*; Collection of Scientific Papers; IGG UrB RAS: Yekaterinburg, Russia, 2006; pp. 379–381. (In Russian)
23. Brown, A.V.; Page, N.J.; Love, A.H. Geology and platinum-group element geochemistry of the Serpentine Hill complex, Dundas Trough, Western Tasmania. *Can. Mineral.* **1988**, *26*, 161–175.

24. Arai, S.; Akizawa, N. Precipitation and dissolution of chromite by hydrothermal solutions in the Oman ophiolite: New behavior of Cr and chromite. *Am. Mineral.* **2014**, *99*, 28–34. [CrossRef]
25. Kapsiotis, A.; Rassios, A.E.; Antonelou, A.; Tzamos, E. Genesis and Multi-Episodic Alteration of Zircon-Bearing Chromitites from the Ayios Stefanos Mine, Othris Massif, Greece: Assessment of an Unconventional Hypothesis on the Origin of Zircon in Ophiolitic Chromitites. *Minerals* **2016**, *6*, 124. [CrossRef]
26. Colás, V.; Padrón-Navarta, J.A.; González-Jiménez, J.M.; Fanlo, I.; Sánchez-Vizcaíno, V.L.; Gervilla, F.; Castroviejo, R. The role of silica in the hydrous metamorphism of chromite. *Ore Geol. Rev.* **2017**, *90*, 274–286. [CrossRef]
27. Dritz, M.; Bochvar, N.R.; Guzei, L.S. *Binary and Multicomponent Copper-Based Systems: Handbook*; Nauka: Moscow, Russia, 1979; 248p. (In Russian)
28. Murzin, V.V.; Varlamov, D.A. Chemical composition of native gold in magnetite ore from the Kagan ultramafic massif (S. Urals). In *Yearbook-Proceedings of the IGG UrB RAS*; IGG UrB RAS: Yekaterinburg, Russia, 2018; Volume 165, pp. 194–199. (In Russian)
29. Wenner, D.; Taylor, H.P., Jr. O/H and O^{16}/O^{18} studies of serpentinization of ultramafic rocks. *Geochim. Cosmochim. Acta* **1974**, *38*, 1255–1286. [CrossRef]
30. Fruh-Green, G.L.; Scambelluri, M.; Vallis, F. O–H isotop ratios of high pressure ultramafic rocks: Implications for fluid sources and mobility in the subducted mantle. *Contrib. Mineral. Petrol.* **2001**, *141*, 145–159. [CrossRef]
31. Murzin, V.V.; Shanina, S.N. Fluid regime and origin of gold-bearing rodingites from the Karabash alpine-type ultrabasic massif, Southern Ural. *Geochem. Int.* **2007**, *45*, 998–1011. [CrossRef]
32. Karpov, I.K.; Chudnenko, K.V.; Kulik, D.A. Modeling chemical mass transfer in geochemical processes: Thermodynamic relations, conditions of equilibria, and numerical algorithms. *Am. J. Sci.* **1997**, *297*, 767–806. [CrossRef]
33. Chudnenko, K.V. *Thermodynamic Modeling in Geochemistry: Theory, Algorithms, Software, Applications*; Academic Publishing House Geo: Novosibirsk, Russia, 2010; 287p, ISBN 978-5-904682-18-7. (In Russian)
34. Kulik, D.A.; Wagner, T.; Dmytrieva, S.V.; Kosakowski, G.; Hingerl, F.F.; Chudnenko, K.V.; Berner, U.R. GEM-Selektor geochemical modeling package: Revised algorithm and GEMS3K numerical kernel for coupled simulation codes. *Comput. Geosci.* **2013**, *17*, 1–24. [CrossRef]
35. Chudnenko, K.; Palyanova, G. Thermodynamic modeling of native formation Cu–Ag–Au–Hg solid solutions. *Appl. Geochem.* **2016**, *66*, 88–100. [CrossRef]
36. Holland, T.J.B.; Powell, R. An internally consistent thermodynamic data set for phases of petrological interest. *J. Metamorph. Geol.* **1998**, *16*, 309–343. [CrossRef]
37. Helgeson, H.C.; Delany, J.M.; Nesbitt, H.W.; Bird, D.K. Summary and critique of the thermodynamic properties of rock-forming minerals. *Am. J. Sci.* **1978**, *278*, 1–229.
38. Robie, R.A.; Hemingway, B.S. *Thermodynamic Properties of Minerals and Related Substances at 298.15 K and 1 Bar (10^5 Pascals) Pressure and at Higher Temperatures*; United States Geological Survey: Washington, DC, USA, 1995; 458p.
39. Tagirov, B.R.; Baranova, N.N.; Zotov, A.V.; Schott, J.; Bannykh, L.N. Experimental determination of the stabilities of Au_2S(cr) at 25 °C and $Au(HS)_2^-$ at 25–250 °C. *Geochim. Cosmochim. Acta* **2006**, *70*, 3689–3701. [CrossRef]
40. Shock, E.L.; Sassani, D.C.; Willis, M.; Sverjensky, D.A. Inorganic species in geologic fluids: Correlation among standard molal thermodynamic properties of aqueous ions and hydroxide complexes. *Geochim. Cosmochim. Acta* **1997**, *61*, 907–950. [CrossRef]
41. Stefansson, A. Dissolution of primary minerals of basalt in natural waters. I. Calculation of mineral solubilities from 0 °C to 350 °C. *Chem. Geol.* **2001**, *172*, 225–250. [CrossRef]
42. Dorogokupets, P.I.; Karpov, I.K. *Thermodynamics of Minerals and Mineral Equilibria*; Nauka: Novosibirsk, Russia, 1984; 186p. (In Russian)
43. Reid, R.C.; Prausnitz, J.M.; Sherwood, T.K. *The Properties of Gases and Liquids*; McGraw-Hill Book Company: New York, NY, USA, 1977; 688p.
44. Sverjensky, D.A.; Shock, E.L.; Helgeson, H.C. Prediction of the thermodynamic properties of aqueous metal complexes to 1000 °C and 5 kb. *Geochim. Cosmochim. Acta* **1997**, *61*, 1359–1412. [CrossRef]

45. Shock, E.L.; Helgeson, H.C.; Sverjensky, D.A. Calculation of the thermodynamic and transport properties of aqueous species at high pressures and temperatures: Standard partial molal properties of inorganic neutral species. *Geochim. Cosmochim. Acta* **1989**, *53*, 2157–2183. [CrossRef]
46. Akinfiev, N.N.; Zotov, A.V. Thermodynamic description of chloride, hydrosulfide, and hydroxo complexes of Ag(I), Cu(I), and Au(I) at temperatures of 25–500 °C and pressures of 1–2000 bars. *Geochem. Int.* **2001**, *39*, 990–1006.
47. Akinfiev, N.N.; Zotov, A.V. Thermodynamic description of aqueous species in the system Cu–Ag–Au–S–O–H at temperatures of 0–600 °C and pressures of 1–3000 bar. *Geochem. Int.* **2010**, *48*, 714–720. [CrossRef]
48. Johnson, J.W.; Oelkers, E.H.; Helgeson, H.C. SUPCRT92: Software package for calculating the standard molal thermodynamic properties of mineral, gases, aqueous species, and reactions from 1 to 5000 bars and 0 to 1000 °C. *Comput. Geosci.* **1992**, *18*, 899–947. [CrossRef]
49. Pokrovskii, V.A.; Helgeson, H.C. Thermodynamic properties of aqueous species and the solubilities of minerals at high pressures and temperatures: The system Al_2O_3–H_2O–NaCl. *Am. J. Sci.* **1995**, *295*, 1255–1342. [CrossRef]
50. Diakonov, I.; Pokrovski, G.; Schott, J.; Castet, S.; Gout, R. An experimental and computational study of sodium–aluminum complexing in crustal fluids. *Geochim. Cosmochim. Acta* **1996**, *60*, 197–211. [CrossRef]
51. Bessinger, B.; Apps, J.A. The Hydrothermal Chemistry of Gold, Arsenic, Antimony, Mercury and Silver. 2003. Available online: http://repositories.cdlib.org/lbnl/LBNL-57395 (accessed on 4 October 2019).
52. Shock, E.L.; Helgeson, H.C. Calculation of the thermodynamic and transport properties of aqueous species at high pressures and temperatures: Correlation algorithms for ionic species and equation of state predictions to 5 kb and 1000 °C. *Geochim. Cosmochim. Acta* **1988**, *52*, 2009–2036. [CrossRef]
53. Chudnenko, K.V.; Pal'yanova, G.A.; Anisimova, G.S.; Moskvitin, S.G. Physicochemical modeling of formation of Ag–Au–Hg solid solutions: Kyuchyus deposit (Yakutia, Russia) as an example. *Appl. Geochem.* **2015**, *55*, 138–151. [CrossRef]
54. Palyanova, G. Physicochemical modeling of the coupled behavior of gold and silver in hydrothermal processes: Gold fineness, Au/Ag ratios and their possible implications. *Chem. Geol.* **2008**, *255*, 399–413. [CrossRef]
55. Zhuravkova, T.V.; Palyanova, G.A.; Chudnenko, K.V.; Kravtsova, R.G.; Prokopyev, I.R.; Makshakov, A.S.; Borisenko, A.S. Physicochemical models of formation of gold–silver ore mineralization at the Rogovik deposit (Northeastern Russia). *Ore Geol. Rev.* **2017**, *91*, 1–20. [CrossRef]
56. Chudnenko, K.V.; Pal'yanova, G.A. Thermodynamic properties of solid solutions in the Ag–Au–Cu system. *Russ. Geol. Geophys.* **2014**, *55*, 349–360. [CrossRef]
57. Yokokawa, H. Tables of thermodynamic properties of inorganic compounds. *J. Natl. Chem. Lab. Ind.* **1988**, *83*, 27–118.
58. Likhachev, A.P. The conditions of magnetite and its ore clusters formation. *Natl. Geol.* **2017**, *4*, 44–53. (In Russian)
59. Zotov, A.; Kuzmin, N.; Reukov, V.; Tagirov, B. Stability of $AuCl_2^-$ from 25 to 1000 °C at pressures to 5000 bar, and consequences for hydrothermal gold mobilization. *Minerals* **2018**, *8*, 286. [CrossRef]
60. Seward, T.M.; Williams-Jones, A.E.; Migdisov, A.A. The chemistry of metal transport and deposition by ore-forming hydrothermal fluids. In *Treatise on Geochemistry*, 2nd ed.; Turekian, K., Holland, H., Eds.; Elsevier: New York, NY, USA, 2014; pp. 29–57.
61. Murzin, V.V. *Gold Mineralization in the Ultramafites of the Urals. Mafic-Ultramafic Complexes of Folded Regions and Related Deposits*; Abstract of the 3D International Conference; Institute of Geology and Geochemistry UB of RAS: Ekaterinburg, Russia, 2009; Volume 2, pp. 61–64.
62. Murzin, V.V.; Sustavov, S.G.; Mamin, N.A. *Gold and Platinum-Group Element Mineralization of Placer Deposits of the Verkh-Neivinsky Massif of Alpine-Type Ultrabasites (the Middle Urals)*; Ural Mining and Geological Academy: Yekaterinburg, Russia, 1999; 93p.
63. Sazonov, V.N.; Murzin, V.V.; Ogorodnikov, V.N.; Volchenko, Y.A. Gold mineralization associated with alpinotype ultrabasites (on the example of the Urals). *Litosfera* **2002**, *4*, 63–77. (In Russian)
64. Zhmodik, S.M.; Mironov, A.G.; Zhmodik, A.S. *Gold-Concentrating Systems of Ophiolite Belts (by the Example of the Sayan-Baikal-Muya Belt)*; Academic Publishing House Geo: Novosibirsk, Russia, 2008; 304p.
65. Paraskevopoulos, G.M.; Economou, M.I. Genesis of magnetite ore occurrences by metasomatism of chromite ores in Greece. *Neues Jahrb. Mineral. Abh.* **1980**, *140*, 29–53.

66. Bakirov, A.G. The relationship between pyrite mineralization and magnetite and sulfide occurrences in ultramafic rocks of the Southern Urals. In *Minerals of Ore Deposits and Pegmatites of the Urals*; UBAS USSR: Sverdlovsk, Russia, 1965; Volume 6, pp. 185–192. (In Russian)
67. Singh, R.N.; Srivastava, S.N.P. Ophiolites and associated mineralization in the Naga Hills, north-eastern India. In *Ophiolites, Proceedings of the International Ophiolite Symposium, Cyprus, Nicosia, 1979*; Panayiotou, A., Ed.; Cyprus Geological Survey: Nicosia, Cyprus, 1980; pp. 758–764.
68. Zucchetti, S.; Mastrangelo, F.; Rossetti, P.; Sandrone, R. Serpentinization and metamorphism: Their relationships with metallogeny in some ophiolitic ultramafics from the Alps. In *Zuffar' Days Symposium in Honor of Piero Zuffardi*; University of Cagliari: Cagliari, Italy, 1988; pp. 137–159.
69. Diella, V.; Ferrario, A.; Rossetti, P. The magnetite ore deposits of the southern Aosta Valley: Chromitite transformed during an alpine metamorphic event. *Ofioliti* **1994**, *19*, 247–256.
70. Agafonov, L.V.; Lkhamsuren, J.; Kuzhuget, K.S.; Oidup, C.K. *Platinum-Group Element Mineralization of Ultramafic-Mafic Rocks in Mongolia and Tuva*; Mongolian State University of Science and Technology: Ulaanbaatar, Mongolia, 2015; 224p. (In Russian)
71. Gahlan, H.A.; Arai, S.; Ahmed, A.H.; Ishida, Y.; Abdel-Aziz, Y.M.; Rahimi, A. Origin of magnetite veins in serpentinite from the Late Proterozoic Bou-Azzer ophiolite, Anti-Atlas, Morocco: An implication for mobility of iron during serpentinization. *J. Afr. Earth Sci.* **2006**, *46*, 318–330. [CrossRef]
72. Einaudi, M.T.; Hedenquist, J.W.; Inan, E.E. Sulfidation state of fluids in active and extinct hydrothermal systems: Transitions from porphyry to epithermal environments. In *Volcanic, Geothermal and Ore-Forming Fluids: Rulers and Witnesses of Processes within the Earth*; Simmons, S.F., Graham, I., Eds.; Society of Economic Geologists Special Publication: Littleton, CO, USA, 2003; pp. 285–314.
73. Barton, P.; Toulmin, J.P. The electrum-tarnish method for the determination of the fugacity of sulfur in laboratory sulfide systems. *Geochim. Cosmochim. Acta* **1984**, *28*, 619–640. [CrossRef]